Gating a Single Cell

Gating a single cell – A label free and real time measurement method for cellular progression

Saw Lin Oo[1], Shishir Venkatesh[1], Abdul-Mojeed Ilyas[1], Vaithinathan Karthikeyan[1], Clement Manohar Arava[1], Eva Yi Kong[2], Chi-Chung Yeung[3], Xianfeng Chen[4], Peter K. N. Yu[2], Vellaisamy A.L. Roy[5]**

[1] State Key Laboratory for THz and Millimeter Waves and Department of Material Science and Engineering, City University of Hong Kong, Kowloon, Hong Kong, S.A.R.

[2] Department of Physics, City University of Hong Kong, Kowloon, Hong Kong, S.A.R.

[3]Department of Chemistry, City University of Hong Kong, Kowloon, Hong Kong, S.A.R.

[4]School of Engineering, Institute for Bioengineering, The University of Edinburgh, King's Buildings, Mayfield Road, Edinburgh, EH9 3JL, United Kingdom.

[5]James Watt School of Engineering, University of Glasgow, G12 8QQ, United Kingdom.

Corresponding authors: Roy.Vellaisamy@glasgow.ac.uk; peter.yu@cityu.edu.hk

ABSTRACT: There is an ever-growing need for more advanced methods to study the response of cancer cells to new therapies. To determine cancer cells' response from a cell-mortality perspective to various cancer therapies, we report a label-free and real time method to monitor the in-situ response of individual HeLa cells using a Single Cell Gated Transistor (SCGT). As a cell undergoes apoptotic cell death, it experiences changes in morphology and ion concentrations. This change is well in line with the threshold voltage of the SCGT, which has been verified by correlating the data with the cell morphologies by scanning electron microscopy and the ion-concentration analysis by ICP-MS. This SCGT could replace patch clamps

to study single cell activity via direct measurement in real time. Importantly, this SCGT can be used to study the electrical response of a single cell to stimuli that leaves the membrane intact.

KEYWORDS: Single Cell Gated Transistor (SCGT); Single cell measurement; Real-time measurement; Label free

Graphical Abstract

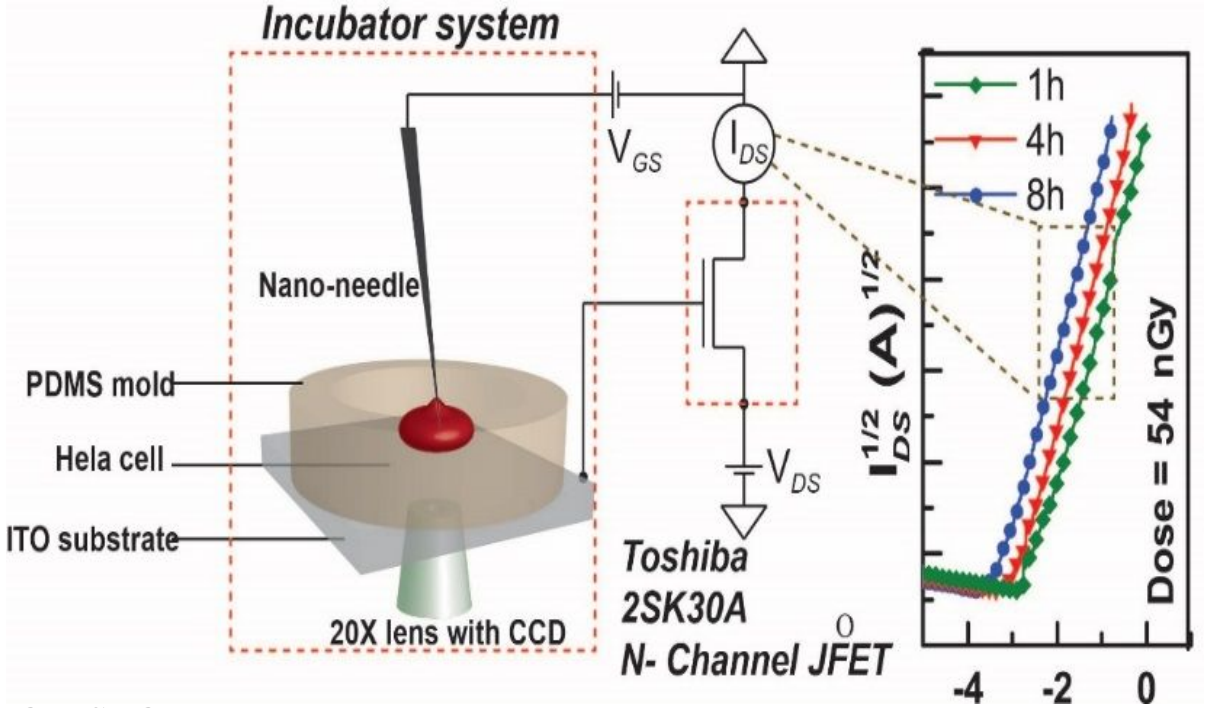

INTRODUCTION

Multi-parameter models from different perspectives are required to understand the noisy and complex responses of single cancer cells to various stimuli. Single cell technology is essentially required for resolving cancer heterogeneity with distinct morphological and phenotypic profiles for individual cells[1]. Singe cell technologies can be classified into single cell separation and single cell analysis. Single cell separation is the basis of cell analysis which provides data of cell's genomic, transcriptomic and proteomic

profiles[2] through methods like optical tweezers, flow cytometry, microfluidics and laser capture micro-dissection (LCM). These approaches have the advantage of averaging out the cellular responses and information, but with an important disadvantage of not covering up the presence of cellular functional subpopulations. Normally, cancer cell death occurs through changes in cell morphology, destruction of ion concentration equilibrium and development of apoptosis bodies followed by cell rupturing[3]. Observation of single cells undergoing apoptosis in real time can provide insights into the metabolic pathways and facilitates to build a conceptual understanding of the whole process. The real time and in situ measurements can help to comprehensively track the changes occurring in live cancer cells over the entire duration of an experiment. Particularly, studying their ion channel activity makes it possible to track the development of apoptotic stages as it provides deep insights in creating a diagnostic tool on how to detect the cancer[4].

For single cell analysis, fluorescence microscopy is a powerful tool which uses labelling tags for molecules to optically track their ion concentration and estimate membrane potential of the cell[5]. Anionic/cationic fluorescent dyes are used as optical indicators which help to understand both the ion channel change and also the membrane potential[6]. However, fluorescence microscopy requires significant cell sample preparation procedures such as cell fixation and permeabilization, cell components extraction, fluorescent tag labelling, making a real-time and in situ monitoring of responses to ionizing radiation impossible[7]. Additionally, the labelling may affect the normal function of cells and ruin the purpose of the study. While fluorescence microscopy is useful in understanding the dynamics of gene expression and transcription, it does not provide a holistic picture of cells[8].

Alternatively, electrical measurements of single cells are commonly achieved through whole-cell patch-clamp methods[9]. In this method, the larger opening of the patch-clamp electrode tip affords the lower resistance and thus better electrical access to the inside of the cells. However, this method results in the complete rupture of the cell-membrane, thereby making long-time interval real-time and in-situ measurements difficult to achieve[10]. Accompanying fluorescence microscopy with measurement of electrical properties of the cells can provide insights into the cell mechanisms such as ion channels and

membrane potential, which are key in explaining cell-fate like cell proliferation, apoptosis and cell division[11].

In order to advance the existing methods of single cell analysis, we have developed a new technique to monitor cells in real time and in-situ to monitor the important parameters related to general behaviour and response to various stimuli at the single cell level. As this proposed method is real-time and in-situ, it is possible to track the cell mortality and determine its progress along the apoptotic stages. This knowledge will enable to monitor the diffusion across ion-channels – an indicator of cell death progression – to design and optimize therapeutic treatment options. The central component to this method is Single Cell Gated Transistor (SCGT) to measure ion concentration changes[12], capacitance and membrane potential changes with a high sensitivity. In our technique, we use a Single Cell gate approach to physically and electrically insulate the electronic transducer FET from the Single Cell gate detector in which biological solutions are placed. The Single Cell Gated Transistor (SCGT) can be placed inside an incubator environment to monitor the activities of living cells for a prolonged time and does not require labelling agents. As such, the SCGT is a promising method for real-time and in-situ analysis of single cells[13].

To verify our technique, we used the SCGT to study the apoptosis process of single HeLa cells via observing the threshold voltage shifts in real-time under in-situ conditions. In addition, the cell morphologies and ion concentrations are recorded with scanning electron microscopy (SEM) and ICP-MS, respectively, followed by establishing a correlation of the data with the threshold voltage shifts from the SCGT. Through the study, we found that the shift in threshold voltage clearly reveals the stage of apoptosis and explains the underlying mechanism of cell death process. Overall, we provide a new technology to conveniently determine single cancer cells' responses to various cancer therapies without the need of using expensive equipment and labelling agents.

EXPERIMENTAL SECTION

General experimental setup. Single cell measurement was carried out by the experimental set up shown in Figure 1(a). Here the ITO-coated glass served as Single Cell gate electrode which is connected to gate terminal of Toshiba 2SK30ATM n-channel JFET. The nano-needle (Naulga **NN-EEUSNP-W500, length 3-5 µm with Parylene "C" coating)** was used to pierce through the cell membrane. All electrical characterization was carried out using Agilent 4155C semiconductor parameter analyzer. The movement of the nano-needle was controlled using micromanipulator stage (Thorlabs RBL 13dl/m). Nikon objective lens with working distance of 3.6 mm and magnification of 20X combined with a Sony (SSC-C370P) colour video camera was used for live imaging of the HeLa cells and the nano-needle. An ^{241}Am alpha-particle source with an activity of 5.02 µCi and average energy of 5.16 MeV was used for cell irradiation[14] and irradiation doses of 27, 54 and 81 nGy is systematically experimented. Prior to irradiation of the cells, the cell concentration was determined using the hemocytometer[15,16]. Subsequent changes in the cell's morphology and its ion concentration change according to the irradiation doses applied are deeply analyzed through SEM and ICP-MS respectively.

Materials. Dulbecco's modified Eagle's essential medium (DMEM), Fetal Bovine Serum (FBS), Trypsin and Phosphate-buffered saline (PBS) solutions (Gibco Grand Island, NY) were purchased from Thermo Fisher Scientific, Hong Kong for cell culture and growth. For substrate modification, 3-aminopropyl triethoxysilane (APTES), 1-ethyl-3-[3-dimethy-laminopropyl] carbodiimide hydrochloride (EDC), and N-hydrox-ysuccinimide (NHS) were purchased from Sigma Aldrich, USA. Sylgard 184 Silicone Elastomer Kit (polydimethylsiloxane) was purchased from Dow Corning, USA.

Cell Culture. HeLa cells obtained from a human epithelial carcinoma cell were grown in Dulbecco's modified Eagle's essential medium (Gibco, Grand Island, NY) with 10 percent Fetal Bovine Serum (FBS) inside the 5 percent carbon-dioxide (CO_2) incubator under constant temperature of 37°C[17].

Substrate Cleaning. Glass substrates coated with 30 ohm/square, indium tin oxide (ITO) were cut into 1.5" squares and cleaned sequentially using 5% Decon 90, ethanol, acetone, and deionized water for 15 minutes each in bath sonicator, followed by drying with high purity nitrogen gas[18].

Preparation of PDMS well on ITO substrate. Sylgard 184 Silicone Elastomer Kit was used for making polydimethylsiloxane (PDMS) wells. First, the uncured resin was mixed homogenously with curing agent in 10:1 weight ratio[19,20]. Then, the mixture was degassed in vacuum (base pressure: 700 mm Hg) to remove bubbles. The clear and homogenous solutions were poured onto molds to create wells with an inside diameter of 12 mm. PDMS was then cured by baking at 85°C for about 30 minutes. The PDMS wells were peeled off from the mold and bonded to the cleaned ITO substrate[21].

Immobilization of HeLa Cells on ITO substrate. The ITO substrates with PDMS wells were cleaned with 100% ethanol and DI water. After drying with nitrogen gas, the samples were subjected to UV-ozone treatment (Jelight Company 144AX-220) for 30 min to generate hydroxide bonds on the surface[18]. Treated ITO substrates were incubated in a solution of APTES in methanol (2%) for 30 minutes to modify the substrates. Then, the modified substrates were treated with a NHS/EDC solution (NHS, 3 $mg \cdot mL^{-1}$; EDC, 2 $mg \cdot mL^{-1}$) for 1 hour at ambient temperature[22] and rinsed with 1X PBS buffer solution to remove the unbound/unreacted molecules[22]. NHS/EDC modified substrates were incubated with a suspension of living HeLa cells in DMEM with 10% FBS inside the 5% CO_2 incubator under constant temperature of 37°C for about 24 h[23]. After incubation, the samples were gently rinsed with copious amount of 1X PBS buffer (< 2mL) to remove the old medium or loosely attached cells. The rinsed samples were kept in growth medium at 37°C for further analysis[24]. Immobilization process of HeLa cells on ITO substrates are shown in Figure 1(b).

Transfer of cells from stock medium to modified ITO-coated glass substrates. To transfer the cells from the cell culture petri-dish to ITO coated glass with PDMS wells, first the medium was removed from the

cell culture petri-dish. Subsequently, the cells were washed by 1X PBS to remove dead cells. Then, the cells were released from the petri-dish by washing with 0.25% trypsin solution for two minutes inside the incubator at 37°C. Then, trypsin was removed and DMEM with 10% FBS was added to the cell suspension. This suspension was diluted to attain a cell concentration of 3×10^4 cells·ml^{-1}. This cell suspension was then transferred onto the modified ITO-coated glass. The substrates were subsequently incubated for 24 hours. The pH throughout the whole experiment was maintained at 7.4 and all the previous steps were performed in the biosafety fume hood[25].

Preparation of unirradiated cells. The "control" unirradiated cells were also left exposed without medium for 1, 2 and 3 min. However, no radiation was applied to these control unirradiated cells. Then 800 µL fresh medium was filled into the PDMS wells. Then substrates were subsequently loaded into the incubator for further characterization.

Sample preparation for Scanning Electron Microscopy. For the SEM analysis, $3x10^4$ cells on plastic tissue cover slips (Thermanox TMX Coverslips) were fixed in 2.5% glutaraldehyde and 2% paraformaldehyde in PBS solution for two hours, washed in PBS for five times (100, 100, 100, 50 and 25%) and two times in double deionized water (100%,100%) for 10 minutes each[26]. After that, samples were dehydrated with increasing concentration of ethanol (30, 50, 70, 80, 90, 95, 100, and 100%). Subsequently, the samples were immersed in the mixture of ethanol and acetone (3:1, 1:1, 1:3), and three times in 100% acetone for 10 min each. After dehydration, the specimens were critical point dried in liquid CO_2 (BAL-TEC CPD 030 Critical Point Dryer) for about one hour. Finally, the specimens were mounted on the aluminium stubs and sputter coated with 10 % Au using BAL-TAC SCD050 instruments[27]. Images were taken by using Phillips XL30ESEM FEG scanning electron microscope at accelerating voltage of 10 kV under vacuum (base pressure: 10^{-5}Pa).

Inductively-coupled plasma mass spectrometry (ICP-MS): This is a technique for the detection of ion concentration in solution[28]. In this work, Optima 2100 DV ICP-OES system was used for potassium ion

(K^+) concentration analysis. Before analysis, $3x10^4$ cells were cultured on each 10 ml petri dish for radiation and control measurements. Samples were kept inside the incubator for 24 h with 5%CO_2 and 37ºC. After 24 h, 3 samples were used for radiation and another 3 samples were used for control measurements. Before irradiation, old medium solution was removed and washed with 1X PBS for removing dead cells and other impurities. After being washed with (2 ml) PBS solution, the cells (3×10^4) were irradiated with the ^{241}Am α-particle source for different periods such as 27 nGy, 54 nGy and 81 nGy. For the control samples, removed the old medium solution from the cell surface, washed with 1X PBS and kept the samples without medium for 1, 2 and 3 min. The medium was collected from both irradiated and control samples for each 1 h, 4 h and 8 h. Finally, the samples were diluted 100 times for potassium ion (K^+) analysis.

RESULTS AND DISCUSSION

Single cell electrical measurements. The real time measurement of single cell is achieved in the SCGT sketched in Figure 1 (a). In the set-up, single cells are first immobilized on an ITO glass substrate via the procedures presented in Figure 1 (b) and then a nanoneedle with a tip diameter of 60 nm will be pierced to a single HeLa cell with a depth of approximately 2.5 μm into the cell membrane with the help of micromanipulator which prevents the nano-needle and ITO substrate to electrically short. The device design is based on our atomic force microscopy (AFM) measurement of the morphological information of HeLa cells (Figure 1 (d-f). During the measurement, HeLa cells are first irradiated to induce apoptosis and the voltage will be constantly monitored to understand the apoptotic pathway mechanism.

Real time measurement of Single Cell Gated Transistor (SCGT) trans-conductance curves is recorded as the gate voltage (V_{GS}) swept from -8 V to 0 V and the drain to source voltage (V_{DS}) is held constant at 10 V. The measurements are carried out inside the incubator with 37°C and 5% CO_2[15] for 8 hours (h) for each of the irradiated (apoptotic cells) and control (living cells) samples. The threshold voltage curves of apoptotic cells and normal healthy living cells present clear difference, as shown in Figure S-1 and S-2 (a, b). The same threshold voltage measurement is subsequently performed for α-particle irradiated HeLa cell

samples with different doses of 27, 54 and 81 nGy. Figure S-2(c-e) shows the change in the threshold voltage curve at different time intervals after irradiation, revealing obvious shift towards negative values with prolonging irradiation time. Furthermore, the real time measurement of the threshold voltage recorded for 8 h signifies the threshold voltage shift between the irradiated and control cell with respect to the doses as shown in Figure 2 (a-c).

The observed shifts in threshold voltage are the response of n-channel JFET from induced positive charges on single cell gate by the irradiated HeLa cell, which is the combined effect of morphology and ion concentration changes[12,31]. However, as one can see, the threshold slope does not change much while the threshold voltage shifts significantly in Figure S-2(c-e). This drastic change in the threshold voltage signifies the increase in the ion transfer across the cell as the morphology changes.

During apoptosis, there is an increased activity in potassium ion channels, leading to increase in efflux of potassium ions and consequently shrinking the cell volume which has been well reported[32]. The change in K^+ ion concentration is hypothesized as the reason behind the shift in threshold voltage as a consequence of increased apoptosis-related activities stimulated by irradiation. The results in Figure 2 collectively explains that the increase in the post-irradiation time leads to the increase in apoptosis-related activities in the cell.

This change in ion concentration influences the V_{GS} and n-channel width or depth due to decreade in depleation layer causing the threshold voltage shift. A mathematical modelling of the threshold voltage with respect to the change in the ion concentration and n-channel width or depth is performed and the results are shown in Figure 3. The finding indicates that the threshold voltage maintains a good linear relation with the ion concentration[33].

Similarly, in Figure 4 (a), we observe that increasing the radiation dose leads to shifting of threshold voltages to negative values. From this, it is inferred that increasing dose leads to increase in apoptosis-

related activities within the cell. The cell death caused by irradiation are counted using a hemocytometer under microscope and the results are shown in Figure 4(b). Over 55% to 60% of the cells are dead upon irradiation doses of 54 and 81 nGy.

Morphological apoptotic changes. HeLa cells in general have a polygonal shape, with the characteristic features of numerous microvilli and lamellipodia extensions, as shown in Figure S-3 (a'-c'). Whereas, the irradiated HeLa cells is observed as spherical in shape with less number of microvilli and small apoptotic bodies present on the cell membrane as shown in Figure 5 (a') and (g'-i'). In our observation, with increase in the irradiation doses, the change in cell surface morphology is obvious which leads to reduced lifetime of the cell. For the irradiation dose of 54 nGy, the stages of development in apoptotic bodies is clearly visible within 1 h and decrease in cell volume is observed after 4 h. At post irradiation time of 8 h, a significant change in their surface morphology with cell shrinkage and increase number of dead cells are observed.

These changes were observed to happen faster at the irradiation dose of 81 nGy and finally 8 h post irradiation, the cells shrink and post-apoptosis debris is seen which confirms the cell death process through apoptosis[29]. This is attributed to the release of potassium ions and formation of apoptotic bodies[30]. These changes in cell morphology stages with change in irradiation doses are clearly shown in the Figure 5. α-particle irradiation induced cell morphology changes with respect to the irradiation dosage and post irradiation time are studied using SEM. The results are shown in Figure 5, while those for the control cells are shown in Figure S-3. Together, these results show the real time and in-situ response of single HeLa cell undergoing apoptosis stages under different dose of α-particle irradiation.

The mechanism responsible for threshold voltage shifts is schematically shown in Figure 6. It can be seen in Figure 6 (a) that an exposure of a HeLa cell to α-particle induces damage to its K^+ ion channels in the plasma membrane, thereby resulting in efflux of K^+ ions and depolarization of the cell membrane[34]. To

compensate for this depolarization, the Na^+ ion channel opens causing the influx of Na^+ ions into the cell[4,30] (Figure 6(b)). However, this influx of Na^+ ions is still smaller than the efflux of K^+ ions, ultimately causing the well-known cellular morphological change termed as "apoptotic volume decrease" (AVD)[4,35,36]. Due to the increase in the concentration of positively charged ions and formation of apoptotic bodies, the threshold curves show negative shift at post irradiation time of 1 and 4 h, as shown in Figure 6 (a',b'). The apoptotic volume greatly decreases after 8 h, thereby increasing the concentration of ions. This progresses into more advanced apoptosis stages and finally results in the formation of apoptotic bodies on the plasma membrane and eventual cell-death[37] (Figure 6(c)). Again, the threshold voltages shift correspondingly to increase in the concentration of positive ions (Figure 6(c')).

The change in the K^+ ion concentration at different post irradiation time were also studied using ICP-MS for each irradiation dosage. The increase in the ion concentration level at different post irradiation time infers to the level of apoptosis. The results from ICP-MS analysis are shown in Figure 7 (a-c) indicates release K^+ ion due to the damage of ion channel after exposure to α-particles. Whereas, the concentration of Ca^+ and Cl^- are in very small traces compared to K^+ ion concentration. These results conclude that K^+ channels play an important role in initiating cell morphological changes and apoptosis-related activities of the cell[36,38,39]. Therefore, the K^+ channel has a role in apoptosis regulation, and it has been proposed as a potential regulator of cancer cell death and a promising anticancer therapy target[40].

CONCLUSIONS

In this work, we developed a method of using SCGT to monitor the apoptosis process of single HeLa cells induced by α-particle irradiation. We observed that the threshold voltages of the SCGT shift towards negative values and the magnitude of this shift maintains a good linear relation with the ion centration and closely associated with the cell morphology change during the apoptosis process. The measurement can be conveniently performed in a cell incubator without needing expensive equipment and labelling agents. With

these advantages, we expect that the small dimensions of the nano-needle combined with the high sensitivity of our SCGT can become a powerful tool for the analysis of single cell responses to various stimuli and facilitate the design of advanced therapies.

ACKNOWLEDGMENTS

We would like to acknowledge Mr. Mike Li and Mr. Daniel Yau for providing technical support to conduct the experiments. We acknowledge the grants from RGC of HKSAR project number T42-103/16N

Competing Interests

The authors declare no competing interests.

ASSOCIATED CONTENT

Supporting information

Supporting information provides additional information on electrical control measurements which supports the ion concentration and morphological changes. Figure (S1) is the control measurement for threshold voltages of Hela cells for 1 min, 2 min and 3 min without radiation. Figure (S2) is the threshold voltages measurements of living cells, dead cells and irradiated cells. The irradiated cells with different doses are plotted the graphs as Figure (S2) (c) to (e). Figure (S3) is the SEM images for the control cells to study the morphologies changes and comparative analysis were approved for irradiated cells morphologies.

REFERENCES

(1) Baslan, T.; Hicks, J. Unravelling Biology and Shifting Paradigms in Cancer with Single-Cell Sequencing. Nat. Rev. Cancer **2017**, 17 (9), 557–569. https://doi.org/10.1038/nrc.2017.58.

(2) Liang, S. B.; Fu, L. W. Application of Single-Cell Technology in Cancer Research. Biotechnol.

Adv. **2017**, 35 (4), 443–449. https://doi.org/10.1016/j.biotechadv.2017.04.001.

(3) Jin, Z.; El-Deiry, W. S. Overview of Cell Death Signaling Pathways. Cancer Biol. Ther. **2005**, 4 (2), 139–163. https://doi.org/10.4161/cbt.4.2.1508.

(4) Bortner, C. D.; Cidlowski, J. A. Ion Channels and Apoptosis in Cancer. Philos. Trans. R. Soc. Lond. B. Biol. Sci. **2014**, 369 (1638), 20130104. https://doi.org/10.1098/rstb.2013.0104.

(5) Svoboda, K.; Yasuda, R. Principles of Two-Photon Excitation Microscopy and Its Applications to Neuroscience. Neuron **2006**, 50 (6), 823–839. https://doi.org/10.1016/j.neuron.2006.05.019.

(6) Johnson, L. V; Walsh, M. L.; Bockus, B. J.; Chen, L. B. Monitoring of Relative Mitochondrial Membrane Potential in Living Cells by Fluorescence Microscopy. J. Cell Biol. **1981**, 88 (3), 526–535. https://doi.org/10.1083/jcb.88.3.526.

(7) Kervrann, C.; Óscar, C.; Sorzano, S.; Acton, S. T.; Unser, M. A Guided Tour of Selected Image Processing and Analysis Methods for Fluorescence and Electron Microscopy. IEEE J. Sel. Top. Signal Process. **2016**, 10 (1), 6–30. https://doi.org/10.1109/JSTSP.2015.2505402.

(8) Sims, P. J.; Waggoner, A. S.; Wang, C.-H.; Hoffman, J. F. Mechanism by Which Cyanine Dyes Measure Membrane Potential in Red Blood Cells and Phosphatidylcholine Vesicles. Biochemistry **1974**, 13 (16), 3315–3330. https://doi.org/10.1021/bi00713a022.

(9) Stephan, G.; Huang, L.; Tang, Y.; Vilotti, S.; Fabbretti, E.; Yu, Y.; Nörenberg, W.; Franke, H.; Göröncsér, F.; Sperlágh, B.; et al. The ASIC3/P2X3 Cognate Receptor Is a Pain-Relevant and Ligand-Gated Cationic Channel. Nat. Commun. **2018**, 9 (1). https://doi.org/10.1038/s41467-018-03728-5.

(10) Ypey, D. L.; DeFelice, L. J. The Patch-Clamp Technique Explained and Exercised With the Use of Simple Electrical Equivalent Circuits. Electr. Prop. Cells **2005**, 1 (615), 1–55. https://doi.org/10.1002/9781118687864.app3.

(11) Ehrenberg, B.; Montana, V.; Wei, M. D.; Wuskell, J. P.; Loew, L. M. Membrane Potential Can Be

Determined in Individual Cells from the Nernstian Distribution of Cationic Dyes. Biophys. J. **1988**, 53 (5), 785–794. https://doi.org/10.1016/S0006-3495(88)83158-8.

(12) Jayant, K.; Porri, T.; Erickson, J. W.; Kan, E. C. Label-Free Electronic Detection of Growth Factor Induced Cellular Chatter on Chemoreceptive Neuron MOS (CvMOS) Transistors. TRANSDUCERS 2009 - 15th Int. Conf. Solid-State Sensors, Actuators Microsystems **2009**, 1814–1817. https://doi.org/10.1109/SENSOR.2009.5285727.

(13) Stern, E.; Steenblock, E. R.; Reed, M. A.; Fahmy, T. M. Label-Free Electronic Detection of the Response. Nano **2008**.

(14) Choi, V. W. Y.; Yum, E. H. W.; Yu, K. N. Micro-Collimator Fabricated by Alpha-Particle Irradiation of Polyallyldiglycol Carbonate Polymer Film and Subsequent Chemical Etching. Nucl. Instruments Methods Phys. Res. Sect. A Accel. Spectrometers, Detect. Assoc. Equip. **2010**, 619 (1–3), 211–215. https://doi.org/10.1016/j.nima.2009.10.120.

(15) Deering, R. A.; Rice, R. Heavy Ion Irradiation of HeLa Cells ’. **1962**, 786, 774–786.

(16) Bernhard, E. J.; Malty, A.; Muschel, R. J. Effects of Ionizing Radiation on Cell Cycle Progression. **1995**, 79–83.

(17) Bischof, H.; Rehberg, M.; Stryeck, S.; Artinger, K.; Eroglu, E.; Waldeck-Weiermair, M.; Gottschalk, B.; Rost, R.; Deak, A. T.; Niedrist, T.; et al. Novel Genetically Encoded Fluorescent Probes Enable Real-Time Detection of Potassium in Vitro and in Vivo. Nat. Commun. **2017**, 8 (1), 1–11. https://doi.org/10.1038/s41467-017-01615-z.

(18) Kim, S. Y.; Lee, J.-L.; Kim, K.-B.; Tak, Y.-H. Effect of Ultraviolet–Ozone Treatment of Indium–Tin–Oxide on Electrical Properties of Organic Light Emitting Diodes. J. Appl. Phys. **2004**, 95 (5), 2560–2563. https://doi.org/10.1063/1.1635995.

(19) Lam, E.; Ngo, T. Manufacturing a PDMS Microfluidic Device via a Silicon Wafer Master. Harvard-MIT Div. Heal. Sci. Technol. HST. J **2007**, 410.

(20) Yang, Y. Lab on a Chip. **2018**, 18 (10). https://doi.org/10.1039/c8lc00088c.

(21) Adly, N.; Weidlich, S.; Seyocka, S.; Brings, F.; Yakushenko, A.; Offenhäussera, A.; Wolfrum, B. Printed Microelectrode Arrays on Soft Materials: From PDMS to Hydrogels. npj Flex. Electron. **2018**, No. December 2017, 1–9. https://doi.org/10.1038/s41528-018-0027-z.

(22) Bart, J.; Tiggelaar, R.; Yang, M.; Schlautmann, S.; Gardeniers, H. Room-Temperature Intermediate Layer Bonding for Microfluidic Devices. **2009**, 3481–3488. https://doi.org/10.1039/b914270c.

(23) Yi, S. As Featured in : Lab on a Chip. **2018**. https://doi.org/10.1039/c8lc00911b.

(24) Tan, H.; Guo, S.; Dinh, N. D.; Luo, R.; Jin, L.; Chen, C. H. Heterogeneous Multi-Compartmental Hydrogel Particles as Synthetic Cells for Incompatible Tandem Reactions. Nat. Commun. **2017**, 8 (1). https://doi.org/10.1038/s41467-017-00757-4.

(25) Carlo, D. Di; Wu, L. Y.; Lee, L. P. Dynamic Single Cell Culture Array. Lab Chip **2006**, 6 (11), 1445. https://doi.org/10.1039/b605937f.

(26) Li, L.; Mak, K. Y.; Shi, J.; Koon, H. K.; Leung, C. H.; Wong, C. M.; Leung, C. W.; Mak, C. S. K.; Chan, N. M. M.; Zhong, W.; et al. Comparative In Vitro Cytotoxicity Study on Uncoated Magnetic Nanoparticles : Effects on Cell Viability , Cell Morphology , and Cellular Uptake. **2012**, 12 (xx), 1–8. https://doi.org/10.1166/jnn.2012.6755.

(27) Dias-lopes, G.; Saboia-vahia, L.; Margotti, E. T.; Fernandes, N. D. S.; Luana, C.; Castro, D. F.; Oliveira-junior, F. O.; Peixoto, J. F.; Britto, C.; Silva-filho, F. C.; et al. Morphologic Study of the Effect of Iron on Pseudocyst Formation in Trichomonas Vaginalis and Its Interaction with Human Epithelial Cells. **2017**, 112 (October), 664–673. https://doi.org/10.1590/0074-02760170032.

(28) Wilbur, S.; Yamanaka, M.; Sannac, S. Characterization of Nanoparticles in Aqueous Samples by ICP-MS White Paper Authors. Charact. nanoparticles aqueous samples by ICP-MS **2015**.

(29) Yoon, S.; Park, S. J.; Han, J. H.; Kang, J. H.; Kim, J. H.; Lee, J.; Park, S.; Shin, H. J.; Kim, K.;

Yun, M.; et al. Caspase-Dependent Cell Death-Associated Release of Nucleosome and Damage-Associated Molecular Patterns. Cell Death Dis. **2014**, 5 (10), e1494-14. https://doi.org/10.1038/cddis.2014.450.

(30) Kondratskyi, A.; Kondratska, K.; Skryma, R.; Prevarskaya, N. Ion Channels in the Regulation of Apoptosis. Biochim. Biophys. Acta - Biomembr. **2015**, 1848 (10), 2532–2546. https://doi.org/10.1016/j.bbamem.2014.10.030.

(31) Chalovich, J. M.; Eisenberg, E. NIH Public Access. Magn Reson Imaging **2013**, 31 (3), 477–479. https://doi.org/10.1016/j.immuni.2010.12.017.Two-stage.

(32) Murakami, T.; Sakata, T.; Matsumoto, A.; Takai, M.; Ishihara, K.; Miyahara, Y. Development of Cell/Transistor Interface for Real-Time and Noninvasive Monitoring of Potassium Ion Release Based on Apoptosis Using Biologically-Coupled Field Effect Transistor. Trans. Mater. Res. Soc. Japan **2010**, 35 (2), 255–258. https://doi.org/10.14723/tmrsj.35.255.

(33) Saha, S. K. Modeling Statistical Dopant Fluctuations Effect on Threshold Voltage of Scaled JFET Devices. **2016**, 507–513.

(34) Kuo, S. S.; Saad, a H.; Koong, a C.; Hahn, G. M.; Giaccia, a J. Potassium-Channel Activation in Response to Low Doses of Gamma-Irradiation Involves Reactive Oxygen Intermediates in Nonexcitatory Cells. Proc. Natl. Acad. Sci. U. S. A. **1993**, 90 (3), 908–912. https://doi.org/10.1073/pnas.90.3.908.

(35) Lang, F.; Hoffmann, E. K. Role of Ion Transport in Control of Apoptotic Cell Death. Compr. Physiol. **2012**, 2 (3), 2037–2061. https://doi.org/10.1002/cphy.c110046.

(36) Kondratskyi, A.; Kondratska, K.; Skryma, R.; Prevarskaya, N. Ion Channels in the Regulation of Apoptosis. Biochim. Biophys. Acta - Biomembr. **2015**, 1848 (10), 2532–2546. https://doi.org/10.1016/j.bbamem.2014.10.030.

(37) Zhang, Y.; Chen, X.; Gueydan, C.; Han, J. Plasma Membrane Changes during Programmed Cell

Deaths. Cell Res. **2018**, 28 (1), 9–21. https://doi.org/10.1038/cr.2017.133.

(38) Li, M.; Xiong, Z.-G. Ion Channels as Targets for Cancer Therapy. Int. J. Physiol. Pathophysiol. Pharmacol. **2011**, 3 (2), 156–166.

(39) Huang, X.; Jan, L. Y. Targeting Potassium Channels in Cancer. J. Cell Biol. **2014**, 206 (2), 151–162. https://doi.org/10.1083/jcb.201404136.

(40) Yu, S. P.; Choi, D. W. Ions, Cell Volume, and Apoptosis. Proc. Natl. Acad. Sci. U. S. A. **2000**, 97 (17), 9360–9362. https://doi.org/10.1073/pnas.97.17.9360.

Figures and Tables

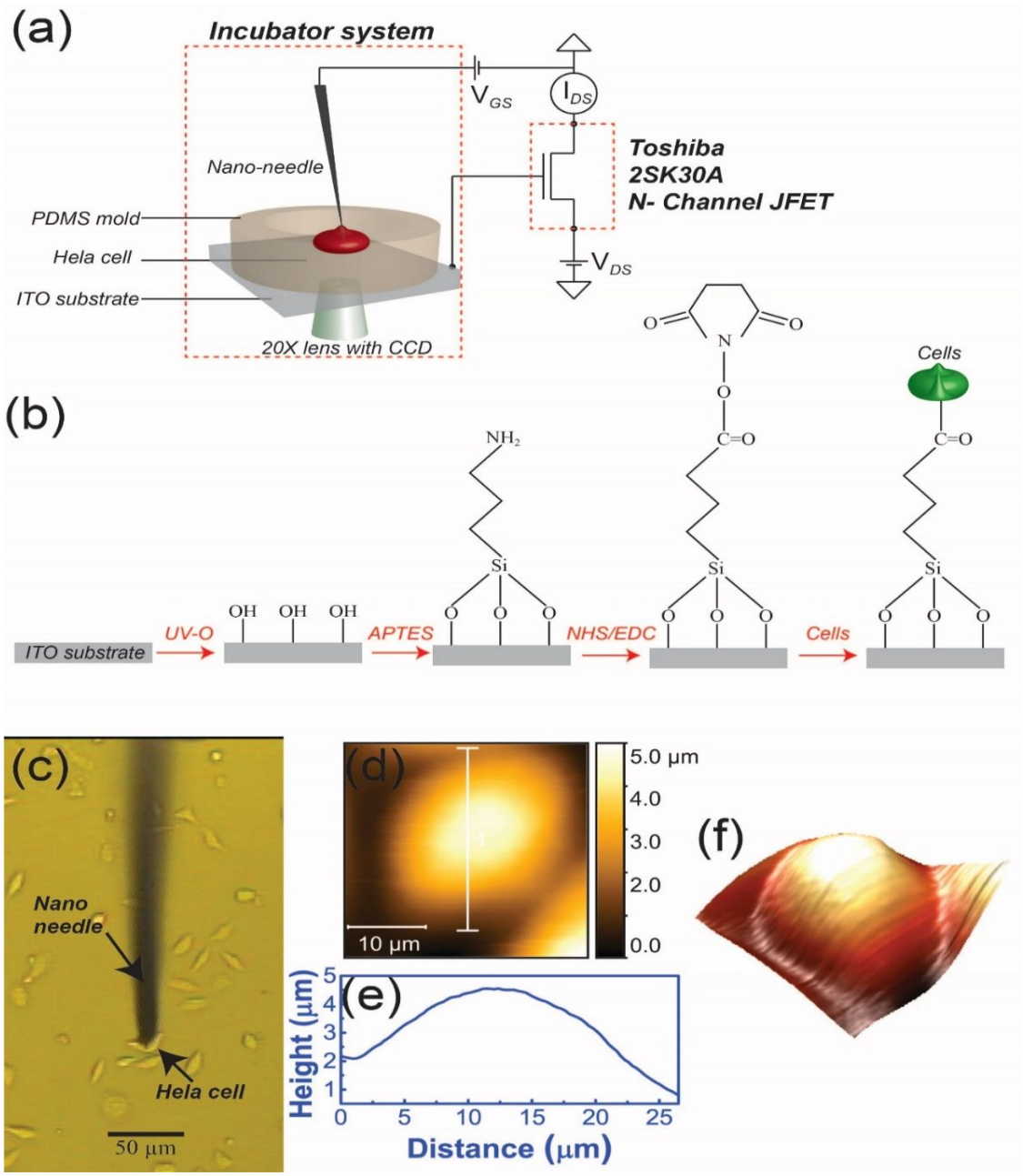

Figure 1 Schematic diagram of the electrical measurement and cell immobilization (a) Transistor based electrical measurement system. **(b)** Cell immobilization process on the ITO electrode. **(c)** Nano-needle for single-cell electrical measurement. **(d)** AFM images for single HeLa Cells. **(e)** Height and distance graph of the single cells AFM analysis. **(f)** AFM 3D images for single HeLa Cells.

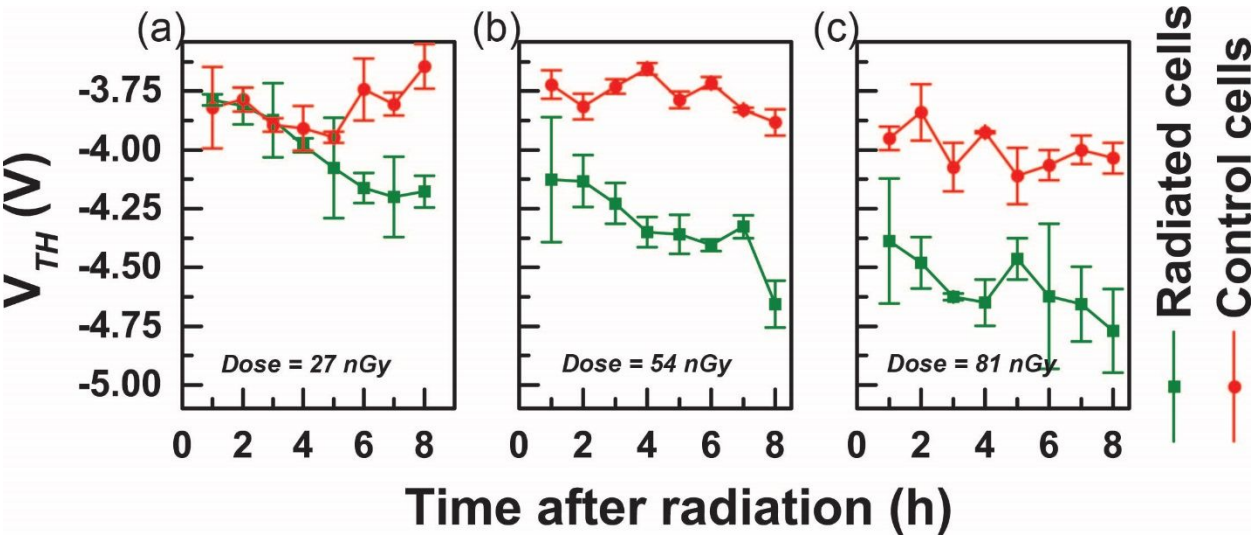

Figure 2 Threshold voltage and time graphs (a) V_{th} and time graph for 27 nGy irradiated cells and control. **(b)** V_{th} and time graph for 54 nGy irradiated cells and control. **(c)** V_{th} and time graph for 81 nGy irradiated cells and their control cells. The statistical analysis was performed on data obtained from three different samples.

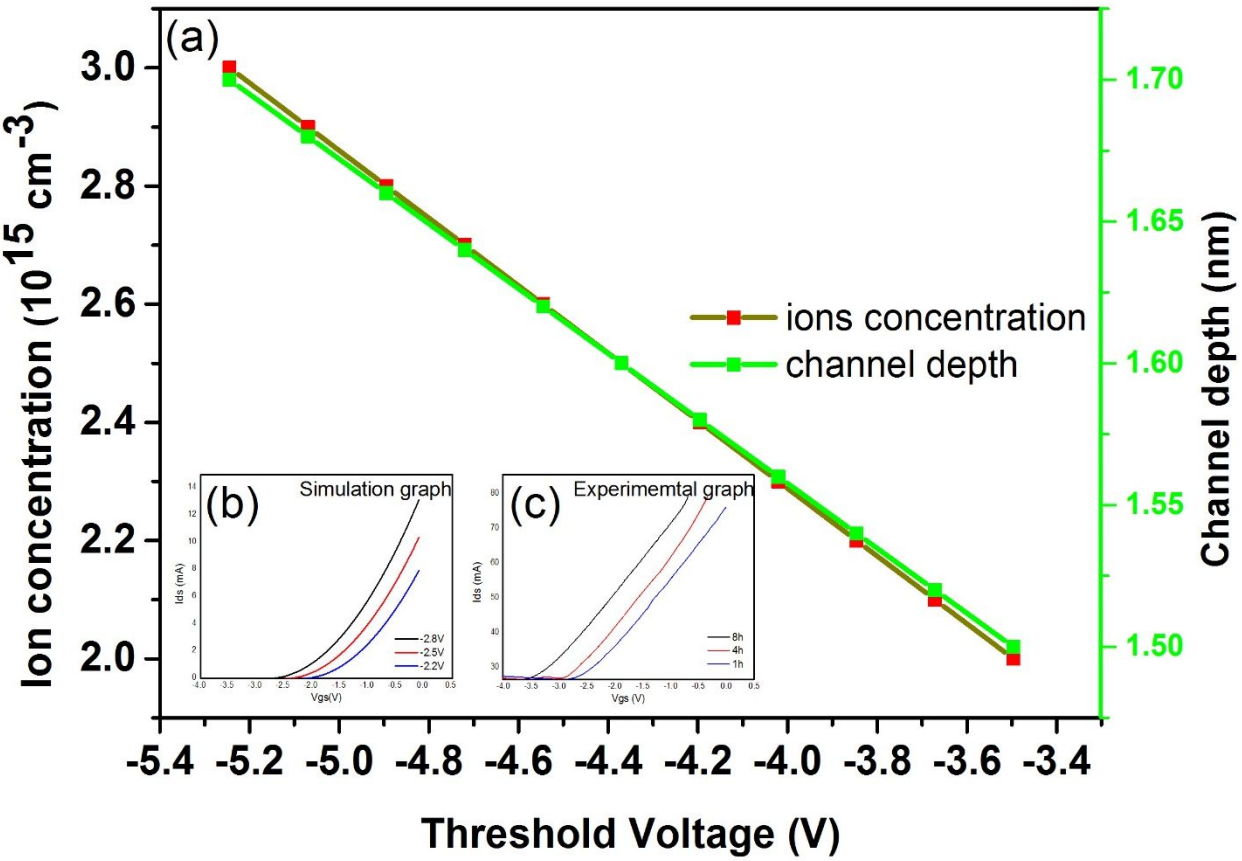

Figure 3. Modelling simulation graph (a) shows the threshold voltage shifts graph with respect to ion concentration and channel width or depth (b) and (c) shows the comparison of experimental and simulated I-V curve.

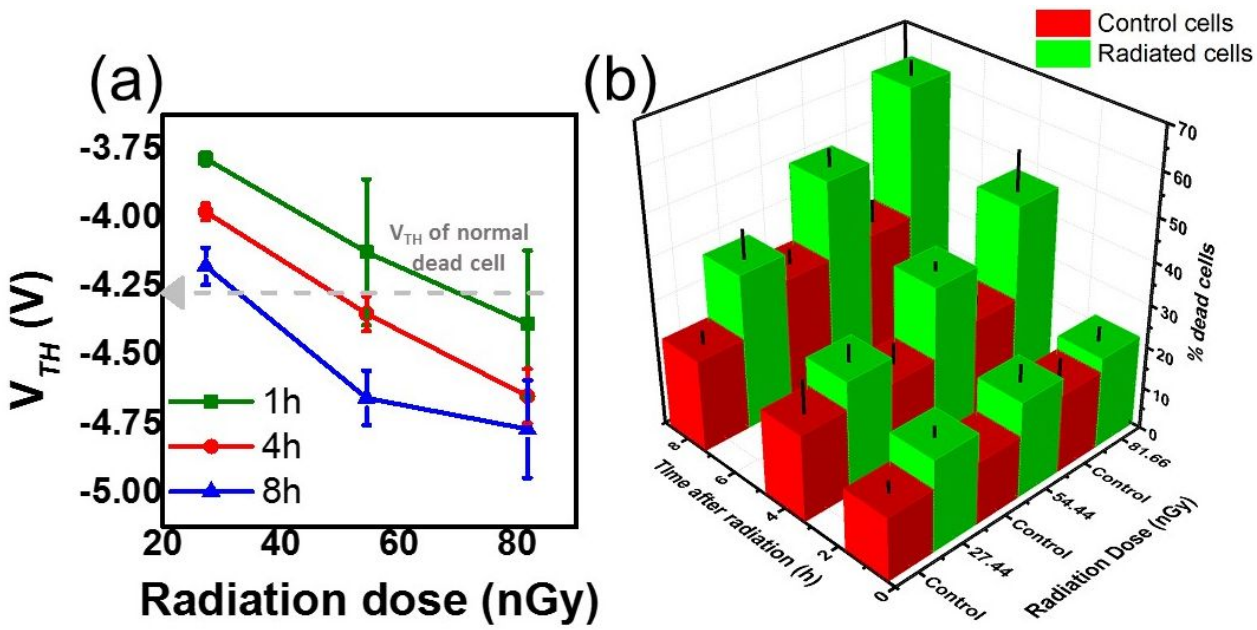

Figure 4 (a) Threshold voltage and radiation dose graph **(b)** Haemocytometer count of dead cells %, with dose rate and time after radiation.

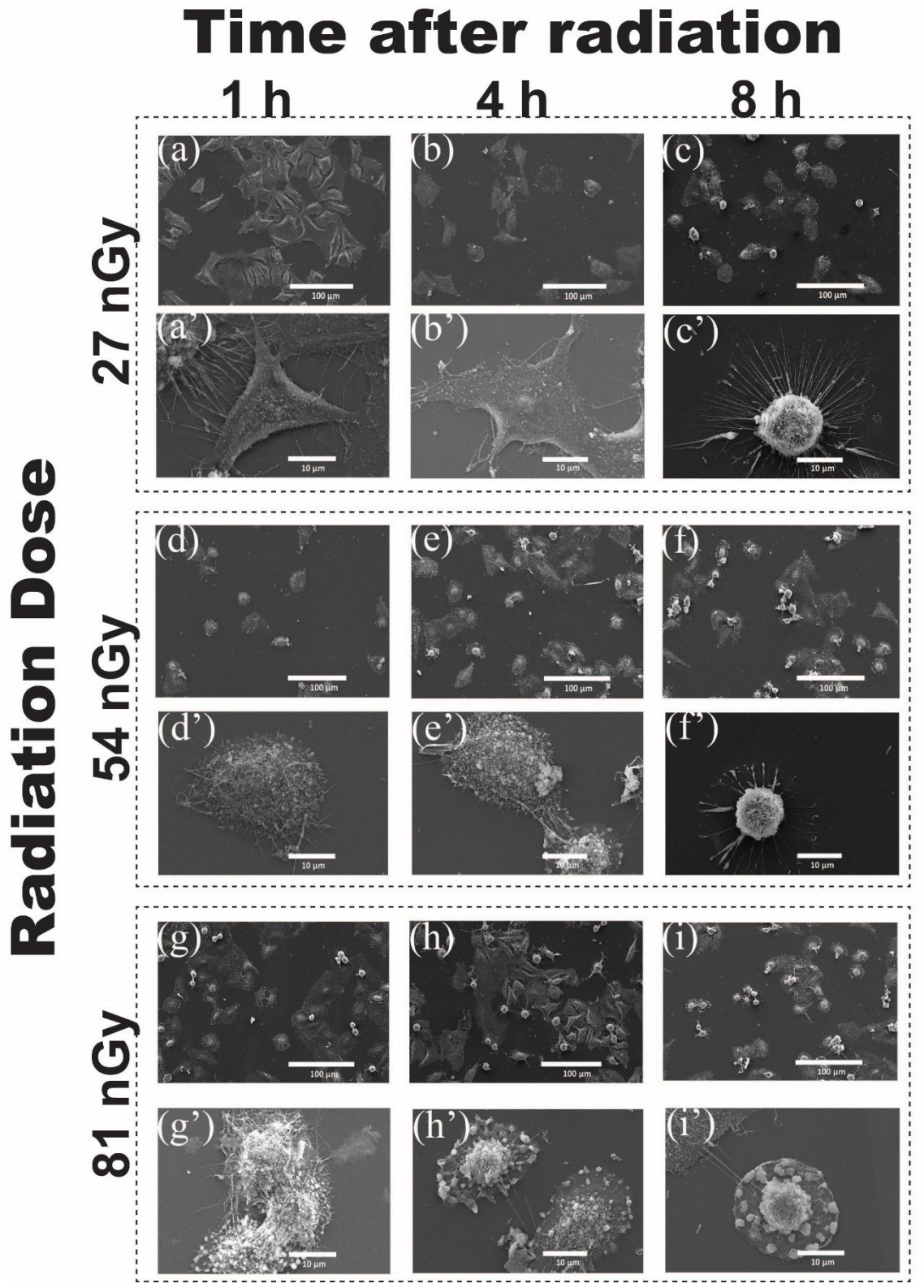

Figure 5 SEM images for irradiated cells (a,a') 27 nGy irradiated cells with 1 hour (h) post irradiation time. (b,b') 1-min (27 nGy) irradiated cells 4 h post irradiation time. (c,c') 27 nGy irradiated cells 8 h post irradiation time.(d,d') 54 nGy irradiated cells 1 h post irradiation time. **(e,e')** 54 nGy irradiated cells 4 h

post irradiation time.**(f,f')** 54 nGy irradiated cells 8 h post irradiation time. **(g,g')** 81 nGy irradiated cells 1 h post irradiation time. **(h,h')** 81 nGy irradiated cells 4 h post irradiation time. **(i,i')** 81 nGy irradiated cells 8 h post irradiation time.

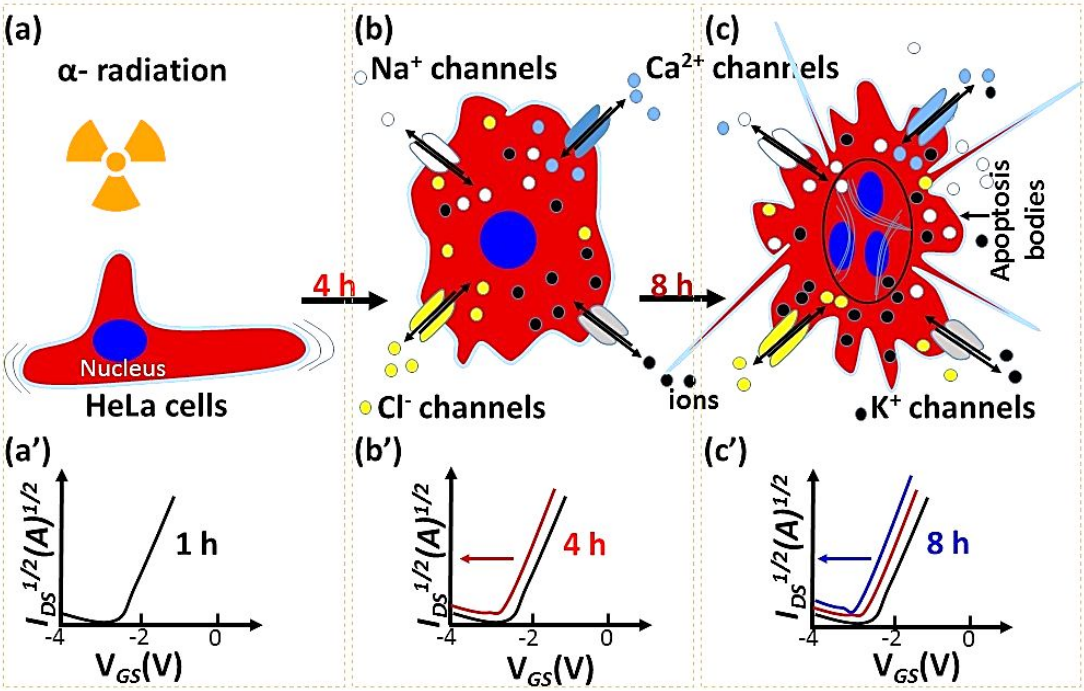

Figure 6 Schematic of mechanism and illustration of threshold voltage shifts due to the ion concentration changes (a) The irradiated HeLa cell and (a') threshold voltage curve within 1 h. (b) The early stage of apoptotic and (b') the threshold curve after 4 h post irradiation time. **(c)** Formation of apoptotic bodies and threshold voltage shift after 8 h post irradiation time **(c')**.

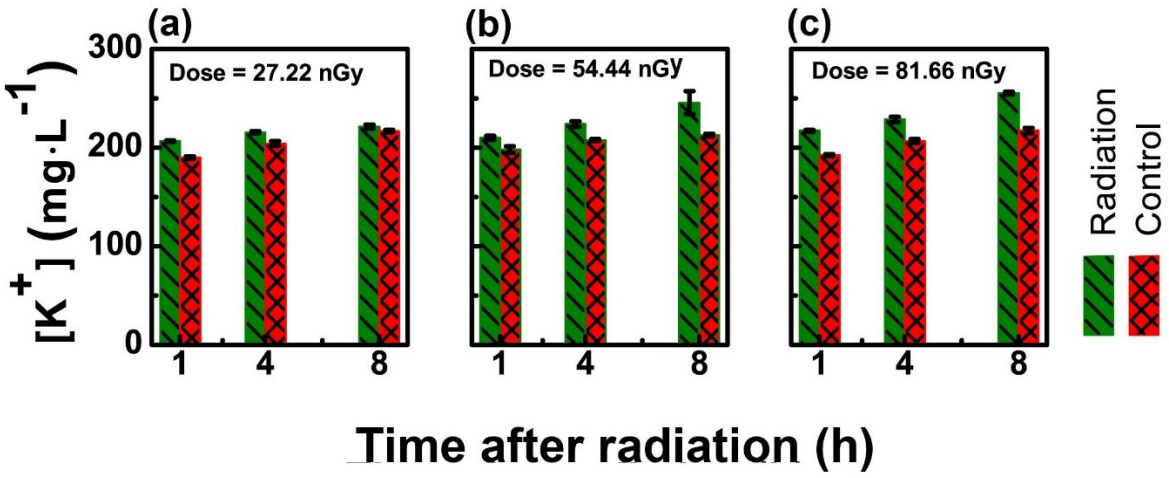

Figure 7 Potassium ion concentration graph (a) Potassium ion concentration for 27 nGy irradiated cells and their control cells. **(b)** Potassium ion concentration for 54 nGy irradiated cells and their control cells. **(c)** Potassium ion concentration for 81 nGy irradiated cells and their control cells.